Simulation of Particle Dispersion in a Two-Dimensional Mixing Layer

Particle dispersion in a two-dimensional mixing layer is analyzed numerically by calculating the particle trajectories in a free shear layer simulated by discrete vortices. Important global and local flow quantities reported in experimental measurements are reasonably simulated.

The particle dispersion results demonstrate that the extent of particle dispersion depends strongly on the Stokes number *St*, the ratio of particle aerodynamic response time to the characteristic time of the mixing layer flow. Particles with relatively small *St* values are dispersed at approximately the fluid dispersion rate. Particles with large *St* values are dispersed at a rate that is less than the fluid rate. Particles with intermediate values of *St* may get flung outside of the vortex structures in the mixing layer and therefore get dispersed at a higher rate than the fluid. This result is in agreement with some previous experiments in plane and axisymmetric jets. It is also found that a higher dispersion rate is associated with the particles introduced to the flow from the low-speed side and from near the middle of the mixing layer.

Reiyu Chein, J. N. Chung
Department of Mechanical and Materials Engineering
Washington State University
Pullman, WA 99164

Introduction

The dispersion of particles by turbulent shear flows is an intrinsic part of many important technological processes. Typical examples include the dispersion of liquid fuel droplets in gas combustors and the mixing of coal particles by the input jets of coal-fired power plants. In many of these processes the dispersion of the particles is a controlling factor in the efficiency and the stability of the process.

The majority of previous predictive efforts for particle dispersion in turbulent shear flows have employed flow-predicting models that involve only the time-averaged properties of the turbulence or have treated the turbulent flow as a random field (Crowe, 1982). Early work by Goldschmidt and coworkers (Goldschmidt and Eskinazi, 1966; Goldschmidt et al., 1972) has shown that turbulent transport increases with particle size based on measured time-averaged particle fluxes and the Fickian gradient diffusion theory. More recently, along the same line of time-averaging approach, concentrated efforts have been devoted to the modeling of particle dispersion with emphasis on the two-way coupling between the two phases in the flow. Encouraging results have been obtained by Elghobashi and Abou-Arab (1983) and Mostafa and Elghobashi (1985), where both the continuous and the dispersed phase are treated by the Eulerian approach and mass, momentum, and energy exchanges between the two phases are included in the model. On the other hand, Faeth and coworkers (Shuen et al., 1983, 1985) have made important contributions both experimentally and theoretically. They adopted numerical models that are based on an Eulerian gas phase and a Lagrangian particle phase. Their numerical predictions match very well with their own experimental results for particle-laden jets.

However, recent developments in the understanding of both bounded and turbulent free shear flows have shown that quasiorderly large vortex structures play a dominant role in the development and momentum exchange of these flows. The revolutionary results of Brown and Roshko (1974) and Winant and Browand (1974) identified the existence of large-scale structures and their mutual interactions. Winant and Browand further indicated that the interactions among the large vortices are responsible for the growth of the mixing layer and they called the merging interactions between two vortices "vortex pairing." These developments in the understanding of the turbulent shear flows have important implications concerning the modeling of particle dispersion in these flows. Recently it was suggested by Crowe et al. (1985) that particle dispersion in free shear layers might be strongly dependent on the ratio of the particle intrinsic aerodynamic response time to the time scale of the large scale

Correspondence concerning this paper should be addressed to J. N. Chung.

vortex structures. This ratio is traditionally called the Stokes number. Based on this physical concept, we expect that particles with relatively small Stokes numbers will disperse at approximately the fluid dispersion rate. Particles at intermediate Stokes numbers may be dispersed more than the fluid and actually be flung out of the vortex structures. Little dispersion is predicted for particles with very large Stokes numbers. This concept offers some explanations for many previous experimental results of increased turbulent transport with increasing particle size (Goldschmidt and Eskinazi, 1966; Householder and Goldschmidt, 1969; Goldschmidt et al., 1972; Lilly, 1973; Memmott and Smoot, 1978; Yuu et al., 1978). Numerical results of Gore et al. (1985), Chein and Chung (1987), and Chung and Troutt (1987) for particle dispersions in a vortex pair and in a jet have also supported this physical concept. It is worth noting that Field (1963) used the same Stokes number concept to explain the results in particle-laden jets that entrainment is increased for flows of very small Stokes number and decreased for large Stokes number.

In this study we investigate the particle dispersion mechanism in a plane mixing layer dominated by large-scale structures. Special emphasis is placed on the effect of large-scale structures on the particle dispersion. The flow field is simulated by a discrete vortex method that has been used successfully in many numerical simulations of shear flows (Acton, 1980; Leonard, 1980; Inoue, 1985). Laitone (1981) adopted the discrete vortex method to study the gas-particle flow over a cylinder. The advantage of applying this method to the study of two-phase flow is that the instantaneous velocity field is applied to the particle motion study, instead of the time-averaged flows. A large number of particles are introduced into the flow field and their trajectories are followed. Thus, in this study, both the flow field and the particle phase are formulated with the Lagrangian approach.

Mathematical Modeling

Flow field simulation

Flow simulation by discret vortices was first introduced by Rosenhead (1932). All the discrete vortex methods that followed contain the basic principles developed by Rosenhead, but each carried its own variations when it came to satisfying the boundary conditions and to conforming to the specific system geometries. Several discrete vortex simulations have appeared in the literature for the two-dimensional turbulent mixing layer. In this study, for flow field simulation we followed basically the method proposed by Inoue (1985), with some of our own improvements. Inoue's method is relatively simple and yet less arbitrary than other simulations. The details of this analysis are as follows.

As shown in Figure 1, the entire flow field is composed of two sections. The first section, corresponding to the flows above and below the splitter plate, is simulated by a vortex sheet of strength Δu per unit length. Δu is defined as,

$$\Delta u = u_1 - u_2 \quad \text{and} \quad u_1 > u_2 \tag{1}$$

where u_1 is the free stream velocity of the top flow and u_2 is that of the bottom flow. In the discrete vortex approximation, this vortex sheet is simulated by an array of equal-strength discrete

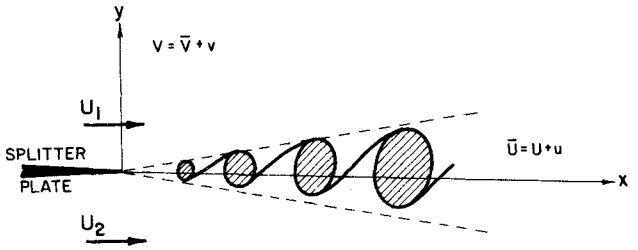

Figure 1. Flow field and definitions.

vortices, each has the strength of Γ as given by,

$$\Gamma = (\Delta u) l \tag{2}$$

where l is the equal spacing between any adjacent vortices. The constant convective velocity of these vortices, u_c, is given by,

$$u_c = \tfrac{1}{2}(u_1 + u_2) \tag{3}$$

The time step in the numerical simulation is chosen such that each vortex moves a distance of l in one time step Δt, therefore,

$$\Delta t = \frac{l}{u_c} \tag{4}$$

It is noted that there is no apparent length scale in a plane mixing layer; l is determined based on the requirement of numerical integration stability. In the current simulation, all the velocities and the lengths are nondimensionlized respectively by a unit velocity $\bar{u}$ and a unit length L. From this point on, the dimensionless quantities are represented by capital letters. τ, the dimensionless time, is defined as $t\bar{u}/L$.

The second section of the flow field corresponds to downstream of the splitter plate, i.e., the mixing layer, which is formed by the vortices shed from the splitter plate. Thus at the beginning of each time step at $X = 0$, one vortex leaves the vortex sheet array of the first section and joins the mixing layer. Once in the mixing layer, the nth vortex moves with a velocity of $\vec{V}_n = (U_n, V_n)$. $\vec{V}_n$ is the summation of all the velocities at the center of this nth vortex (X_n, Y_n) induced by all other vortices in the system plus its own convection velocity U_c. In terms of a complex potential $W(Z)$, we may define

$$U_n - iV_n = \frac{\partial W}{\partial Z} \quad \text{and} \quad Z_n = X_n + iY_n \tag{5}$$

and

$$W(Z_n) = \sum_{k=1}^{N_b} \frac{i\Gamma_k}{2\pi} \ln (Z_n - Z_{bk}) + U_c Z_n + \sum_{\substack{j \neq n \\ j=1}}^{N_m} \frac{i\Gamma_j}{2\pi} \ln (Z_n - Z_j) \tag{6}$$

In the above equation, the first term on the righthand side is due to the contribution from all the vortices in the first section of the vortex sheet. N_b is the total number of vortices that represent the vortex sheet. In this analysis N_b is equal to 600. N_b was determined based on trial and error and it was found that any larger N_b did not change the results significantly. Z_{bk} represents the location of the ith vortex in the vortex sheet array. The second

term corresponds to its own convective velocity. The third term represents the influence from vortices in the second section where N_m is the total number of vortices in the second section of the flow field. The movement of vortices in the mixing layer is determined by

$$\frac{dX_n}{d\tau} = U_n$$

$$\frac{dY_n}{d\tau} = V_n \tag{7}$$

If (X_n^k, Y_n^k) is the position of the nth vortex at the kth time step, then its location at the $(k+1)$th time step, (X_n^{k+1}, Y_n^{k+1}), is calculated based on the first-order Euler's method as follows:

$$X_n^{k+1} = X_n^k + U_n(X_n^k, Y_n^k)\Delta\tau$$
$$Y_n^{k+1} = Y_n^k + V_n(X_n^k, Y_n^k)\Delta\tau \tag{8}$$

where $\Delta\tau$ is the dimensionless time step. The reason for adopting the first-order Euler's method is based on the availability of computing time and the reasonable comparison of the numerical results with the experimental measurements.

Particle dispersion

Particle transport in the mixing layer is visualized by following the movement of each particle in the flow. The trajectory of each particle in the flow is predicted directly from the equation of motion. The basic assumptions in the particle motion analysis are:

1. All the particles are rigid spheres with diameter d_p and density ρ_p
2. The density of the particles is assumed to be large compared to the density of the fluid
3. Particle-particle interactions are neglected
4. A dilute two-phase particle flow is assumed and therefore the effect of the particles on the flow is neglected

Based on the above assumptions it is generally accepted that the dominant force on each particle is the drag force from the ambient fluid. Consequently, forces on the particles such as the virtual mass force, pressure gradient force, and Basset force are neglected in this model.

The nondimensional equation of motion for a particle according to the length and velocity scales chosen above can be written as

$$\frac{d\vec{V}_p}{d\tau} = \frac{f}{St}(\vec{V} - \vec{V}_p) \tag{9}$$

where $\vec{V}_p$ is the dimensionless instantaneous particle velocity, $\vec{V}$ is the dimensionless instantaneous velocity of the fluid, f is the correction factor for any deviation from the Stokes drag, and St is the Stokes number, which is defined as the ratio of particle aerodynamic response time to the flow field time scale:

$$St = \frac{\frac{\rho_p d_p^2}{18\mu}}{\frac{L}{\bar{u}}} \tag{10}$$

μ is the fluid dynamic viscosity. The factor f is well represented for particle Reynolds numbers less than 1,000 by

$$f = 1 + 0.15\, Re_p^{2/3} \tag{11}$$

where Re_p is defined as

$$Re_p = \frac{|\vec{v} - \vec{v}_p| d_p}{\nu} \tag{12}$$

ν is the fluid kinematic viscosity. With the introduction of the flow field Reynolds number $Re_f = \bar{u}L/\nu$, and the nondimensionalized particle size $\gamma_d = d_p/L$, Eq. 12 can be rewritten as

$$Re_p = \left|\vec{V} - \vec{V}_p\right| \gamma_d Re_f \tag{13}$$

In Eq. 10 the Stokes number is related to the flow field Reynolds number, to the density ratio $\gamma_\rho = \rho_p/\rho$, where ρ is the fluid density, and to the nondimensional particle size γ_d, by the following:

$$St = (1/18)\gamma_d^2 \gamma_\rho Re_f \tag{14}$$

The density ratio for gas-particle and gas-liquid droplet flows ranges from 800 to 3,000. For these types of flows, the Stokes number, St, is usually of the order of unity, however, it could vary from as little as 10^{-1} to as large as 10^4 depending on the size and density of the particles. Since the flow simulation is based on the assumption of a large Reynolds number inviscid flow, the choice of flow Reynolds number should be consistent with the flow assumption. In this analysis, the Reynolds number of the flow field is set at 200,000. It is important to note that the Reynolds number is only involved in the drag calculation for particle motion that is generally in the low Reynolds number category where the viscosity is essential; it is not involved in the flow simulation, because the mixing layer has been shown experimentally to be relatively independent of viscosity and dominated by large-scale structures. Also, the density ratio γ_ρ is set at 1,000 to represent a two-phase flow of solid-particle and gaseous fluid.

It should be noted that according to Eq. 14, for a given set of Reynolds number and density ratio each St corresponds to a specific γ_d. Therefore, there is a one-to-one correspondence between the St and the γ_d in this calculation if Re_f and γ_ρ are fixed.

Results and Discussion

Flow field development

The input parameters used in the simulation are given as follows,

$$\alpha = \frac{U_2}{U_1} = 0.6, \quad \lambda = \frac{U_1 - U_2}{U_1 + U_2} = 0.25$$

$$\Delta U = 1.6$$

In order to ensure numerical convergence, the time step must be sufficiently small. In this simulation, the time step $\Delta\tau = 0.1$ was chosen and was found to provide stable numerical integration.

As indicated in Eq. 6, unreasonably large velocities would be induced at each other's positions if two vortices were to get very close to one another. These induced large velocities do not exist in reality because of the viscous effects. In the inviscid discrete vortex approach, Chorin (1973) suggested the concept of vortex blobs with a finite core size to alleviate the singularity problem. We adopt his model in the current analysis. In the current study,

each vortex blob is assigned the following stream function:

$$\psi = \begin{cases} (\Gamma/2\pi) \ln r, & r \geq \sigma \\ \Gamma r/2\pi r, & r < \sigma \end{cases} \tag{15}$$

where r is the distance from the center of the vortex blob and σ is the cutoff radius. It is noted that the introduction of a cutoff radius does not affect the induced velocity outside the cutoff range. We have found that if σ is relatively small, the flow calculation is not sensitive to the choice of σ. In the current analysis σ is equal to $0.6l$.

At the beginning of the flow development in the mixing layer, the flow field evolution is similar to the roll-up of a vortex sheet. As a result, a leading large swirl of concentrated vortices is formed. This leading large vortex structure is moving downstream at a relatively constant velocity approximately equal to u_c. The influence of the leading roll-up structure on the development of the mixing layer between $X = 0$ and $X = 200$ is negligible when $\tau > 120$. After that the mixing layer of interest ($0 < X < 200$) is considered fully developed and quasisteady because stable mean velocity profile and velocity similarity have been established.

In Figure 2, the development of a mixing layer in time is shown at a constant interval of time. The dashed lines indicate the locations of a vortex structure at two different times. When two dashed lines converge, it means that the two corresponding structures are merging into a single but larger vortex structure. This is the so-called pairing process as described by Winant and Browand (1974). Figure 2 is also similar to the x-t diagram in the study of Roshko (1976). It is plausible to assume that there are three distinct regions in the fully developed mixing layer. Immediately following the starting point of the mixing layer

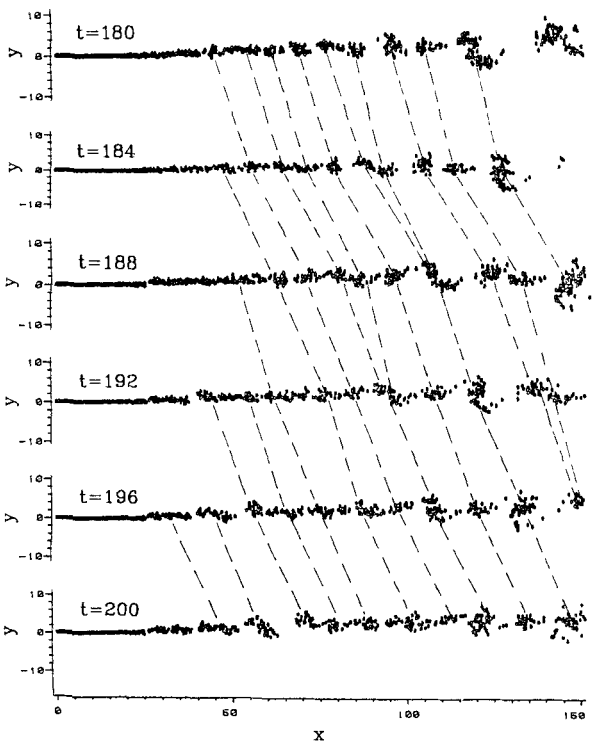

Figure 2. Developments of flow field at various stages.
——— Movements of large-scale structures

($X = 0$) and up to about $X = 60$, it is the region of the onset of nonlinear instabilities and transition to turbulence. Between $X = 60$ and $X = 90$, clusters of vortices are formed due to the roll-up of vortices and breakup of the roll-up vortex structures from the unstable vortex sheet. For the next region, clusters are interacting with neighboring structures. First they rotate around each other and then gradually they merge to form a single larger vortex structure and lose their individual identities. We may call this region the pairing region. After the primary pairing, further pairing between these large vortex structures formed from the primary pairing will occur; such merging will create even larger, secondary vortex structures. This process may continue, but in actual flows a three-dimensional stretching effect will set in and the ordered large-scale structure will cease to exist. The current study is centered on the relatively young mixing layer region ($X = 0$ to $X = 200$), which is basically dominated by the two-dimensional large-scale vortex structures.

In addition to the successful simulations of the global features observed in the experiments, the numerical model has been further evaluated through the comparison of the predicted results with the experimental measurements for the time-averaged local flow quantities. For three downstream locations the mean streamwise velocity profile, the turbulent intensities in both x and y directions, and the Reynolds stress were calculated and compared by Chein (1986) with the experimental results of Oster and Wygnanski (1982). The momentum thickness as a function of downstream location was also calculated and compared with that measured by Oster and Wygnanski. Reasonably good agreements are shown in those comparisons. Self-preservations of all quantities are also confirmed by overlapping the profiles from three downstream locations. In view of both the qualitative and quantitative comparisons, we feel that the flow solutions are reasonably accurate and adequate for the particle dispersion study.

Particle dispersion

In this study we will focus on the particle dispersion in the fully developed flow field; therefore, particles are introduced into the flow field after $\tau = 120$. For convenience, we redefine a new time scale, $T = \tau - 120$, in which $T = 0$ corresponds to $\tau = 120$. The particle initial velocities are assumed to be equal to the local fluid velocities. The assumption that the particle is in dynamic equilibrium with the flow is based on the experimental measurements of Yuu et al. (1978).

Before we address the statistical quantities of particle dispersion in a mixing layer, a discussion of the entrainment of particles due to turbulent flow is helpful. Perhaps the best way to achieve this purpose is to study the particle streaklines at any instant and the particle trajectories throughout the flow field of interest. The typical streakline plots for various Stokes numbers at $T = 70$ are shown in Figure 3. In order to examine the differences in particle streaklines as a function of particle starting positions, particles are released separately from the high-speed side, the low-speed side, and near the origin of the splitter plate. Specifically in the numerical simulation, the particles are released from five vertical locations, $(X, Y) = (0, -4)$, $(0, -2)$, $(0, 0)$, $(0, 2)$, and $(0, 4)$. For the convenience of examination, the streaklines are plotted separately according to the locations at which particles were released. In this analysis, particles with a Stokes number of 0.1 are regarded as equivalent to the fluid particles. This is substantiated by the particle distribution pattern

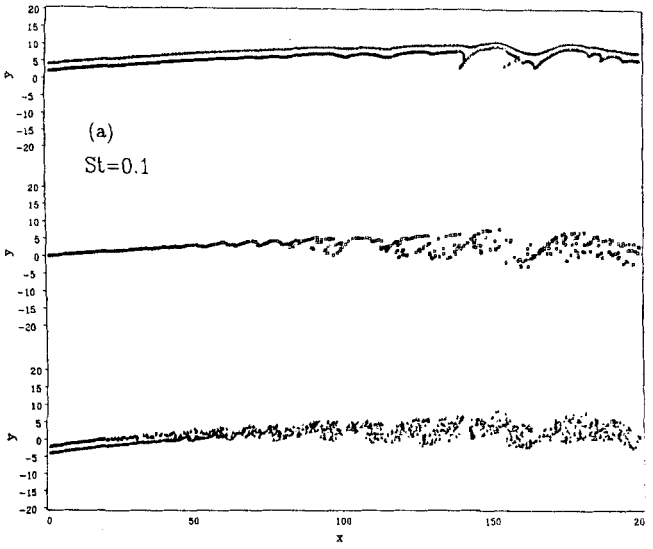

Figure 3a. Particle streakline plots, St = 0.1.

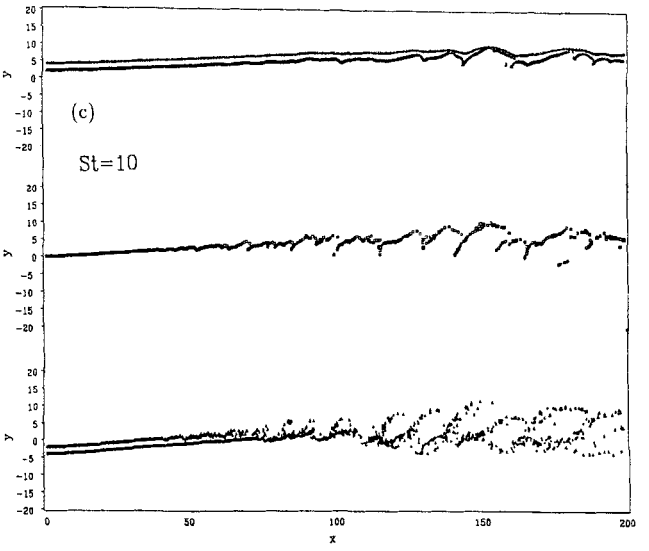

Figure 3c. Particle streakline plots, St = 10.

shown in Figure 3a. It can be seen that the particle distribution patterns for St = 0.1 closely resemble those of large-scale vortex structures shown in Figure 2. The particles released in the high-speed side usually get entrained into the mixing layer by a large-scale vortex structure from its downstream side (right of the vortex cluster) while the particles coming from the low-speed side join the vortex structure from the upstream side. This mixing mechanism is due to the clockwise rotation pattern of the large-scale vortices in the current arrangement (high-speed flow is on top of the low-speed flow). For large Stokes numbers (>50 in our analysis), particles are hardly entrained by the large-scale structures in the mixing layer and they all follow almost linear trajectories with small zig-zag fluctuations.

In general, the particle dispersion patterns for the particles released in the high-speed side are quite different from those released in the low-speed side for a given Stokes number. The differences are attributed to the intrinsic local effective Stokes numbers. Because of the higher local fluid velocity, the intrinsic Stokes numbers of the upper stream particles are larger than those for the lower stream particles even though a unique nominal Stokes number is defined for the entire mixing layer. The following discussion is more directed at the lower stream particles because of their relatively larger dispersion rates in the mixing layer. As we increased the Stokes number to 1, the dispersion picture in Figure 3b is quite different from that of St = 0.1 in Figure 3a. As shown in Figure 3b, some of the particles get flung out of the large-scale vortex structures. In general, particles move away from the cores of large vortex structures and almost particle-free core regions result. As we move to St = 10 the pattern remains similar to that of St = 1 but particles get flung further out from the centers of these large-scale structures. For even higher St, particle dispersion patterns start to switch to a different form which shows less particle dispersion and less influence of particles by the flow. At St = 500 even the lower stream particles also follow an almost straight path. The higher dispersion patterns seem to be more persistent for par-

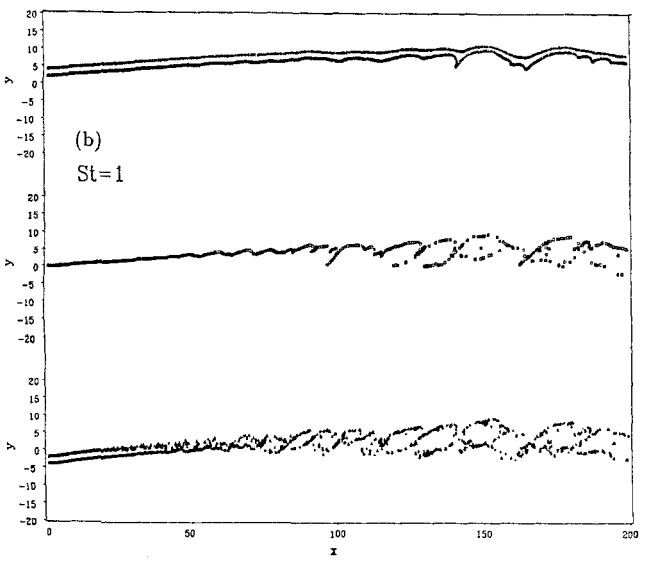

Figure 3b. Particle streakline plots, St = 1.0.

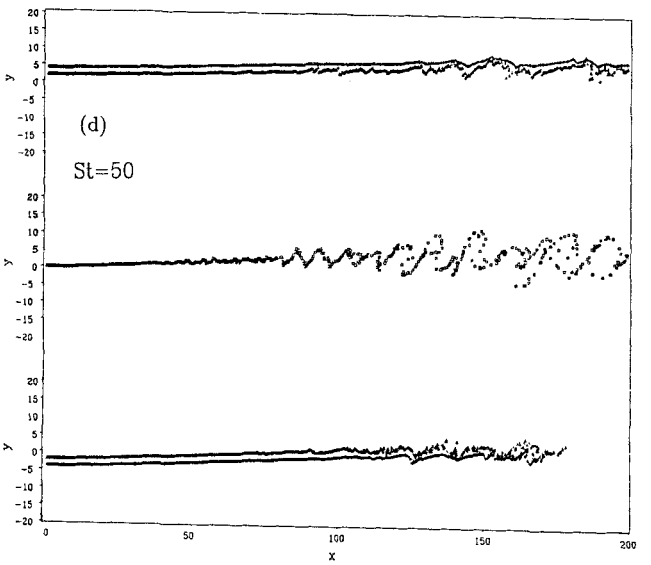

Figure 3d. Particle streakline plots, St = 50.

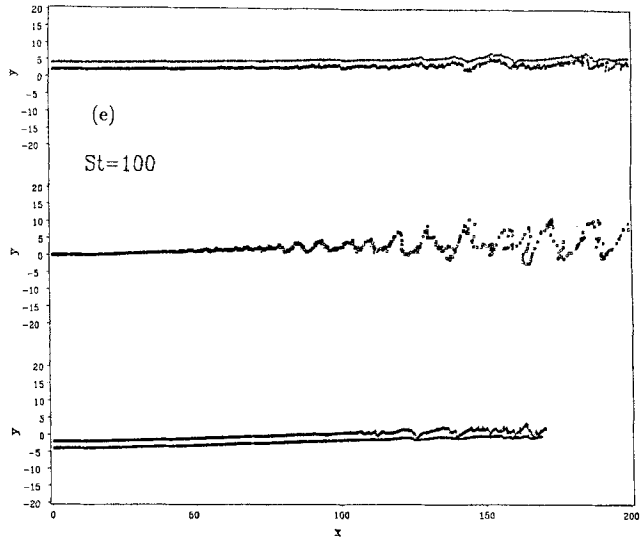

Figure 3e. Particle streakline plots, St = 100.

ticles released near the splitter plate. This is mainly due to the fact that these particles have more time to interact with the mixing layer before being flung out. In summary, the dispersion will increase with increasing Stokes number up to a range of intermediate Stokes numbers. After that, the dispersion will decrease sharply as Stokes number is increased further.

Some typical particle trajectories through the flow field are shown in Figure 4 for various particle Stokes numbers. Equal numbers of particles are released from the high-speed side and the low-speed side. Their trajectories are then traced until they leave the computation domain, i.e., $X = 200$. It is as expected that the trajectories for particles of small Stokes numbers are more complicated than those of large Stokes numbers. For those with large Stokes numbers, particle trajectories are almost linear. Due to the rapid mixing in the low-speed region, it is also seen that the trajectories of particles issued from the low-speed side change more rapidly than those issued from the high-speed side.

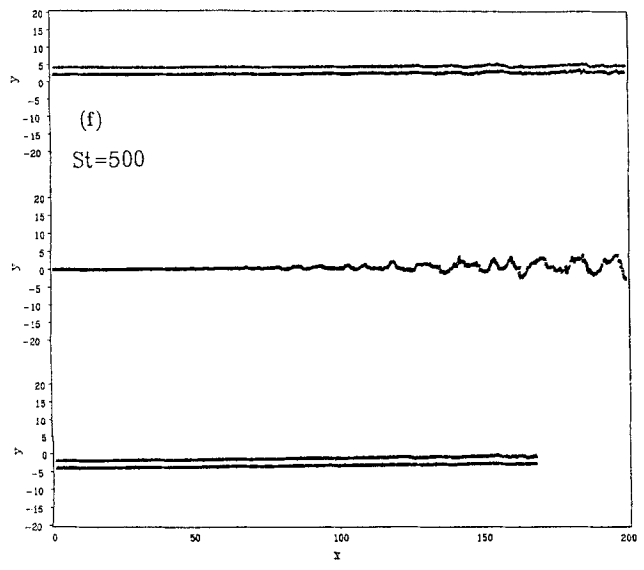

Figure 3f. Particle streakline plots, St = 500.

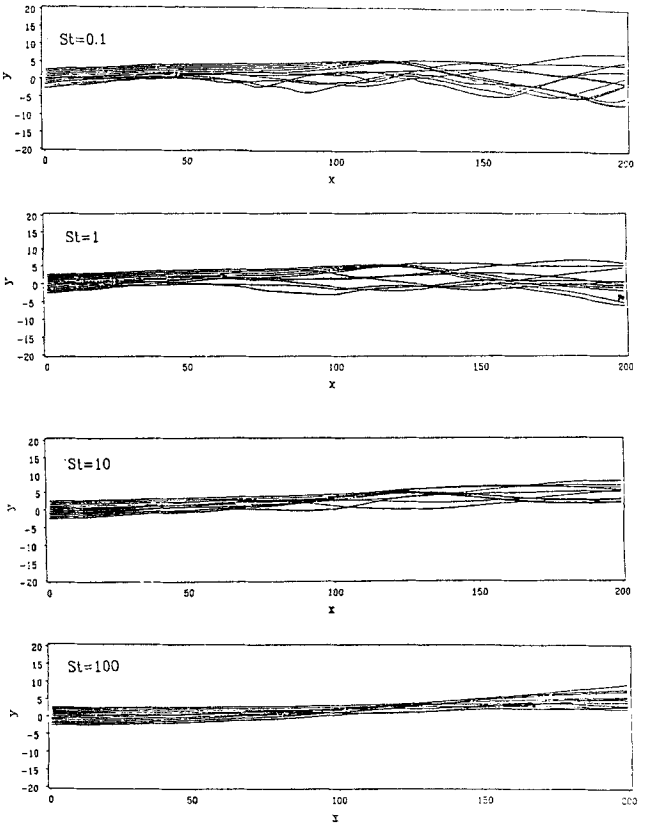

Figure 4. Typical particle trajectories throughout the flow field of interest.

From the above discussion, we realized that the mixing of particles in a shear layer also depends on the locations from which they are introduced into the flow field. In the calculations of the statistical quantities for particle dispersion, we need to establish a uniform line source that is perpendicular to the splitter plate near $X = 0$. In this way, the particles released from the high-speed side, from the low-speed side, and near the origin of splitter plate can all be taken into consideration.

The line source of particles, which is perpendicular to the splitter plate, is represented by five discrete point sources. Starting from $T = 0$ ($\tau = 120$), one particle is released from each point source at every time step continuously, until $T = 60$. Therefore, after $T = 60$ the total number of particles in the flow field is 3,000. The statistical quantities, such as the particle time-averaged velocities, particle distribution, and dispersion, are obtained from the individual status of these 3,000 particles.

First we present the comparison of the time-averaged particle velocity with the time-averaged fluid velocity. The results are shown in Figure 5 for $St = 1$ and $St = 10$. At these Stokes numbers, particles start to get flung out of the vortex structures. If the particles get flung out from the top half of the vortex (high-speed side), they generally wind up being ahead and moving faster than the vortex. If they get flung out from the bottom half (low-speed side), they generally get thrown in the opposite direction relative to the vortex motion. This explains that particles move faster than the fluid in the high-speed side and slower in the low-speed side. Experimentally, the same results were also obtained by Yuu et al. (1978) in the measurements of gas-particle two-phase jets.

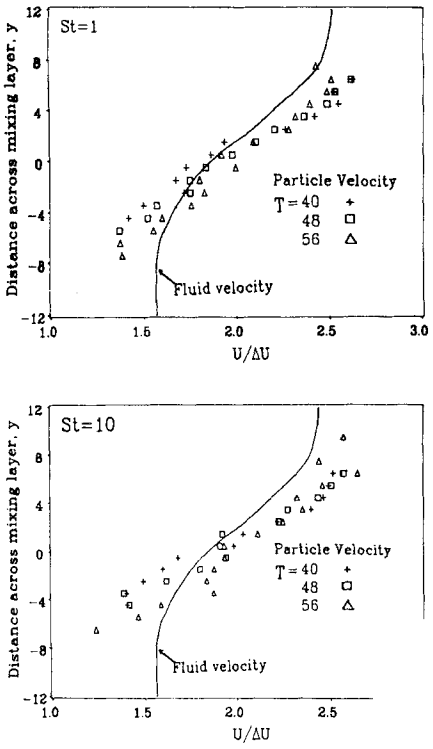

Figure 5. Time-averaged velocities of particles and fluid.

In most applications, the particle dispersion in the direction lateral to the flow stream is of interest. As an attempt to quantify the results concerning the particle lateral dispersion, the lateral dispersion function at time T is defined following Batchelor (1956),

$$D_y^2(T) = \frac{1}{N(T)} \sum_{i=1}^{N(T)} [Y_i(T) - Y_m(T)]^2 \tag{19}$$

and

$$Y_m(T) = \frac{1}{N(T)} \sum_{i=1}^{N(T)} Y_i(T) \tag{20}$$

where $N(T)$ is the total number of particles in the flow field at time T. $Y_i(T)$ is the lateral position of the ith particle at time T. $Y_m(T)$ is the mean value of particle lateral positions at time T.

To compare the dispersion of particles with that of the fluid in a mixing layer, tagged fluid particles are introduced to the mixing layer in a format identical to those of actual particles as described above. The dispersion function of such fluid particles is similarly defined by Eq. 19 and denoted as $D_{fy}^2(T)$. We define the ratio $\gamma_D(T)$ as:

$$\gamma_D(T) \equiv \frac{D_y^2(T)}{D_{fy}^2(T)} \tag{21}$$

$\gamma_D(T)$ represents the particle dispersion as compared to the fluid dispersion at a specific time T. $\gamma_D(T)$ may be thought as similar to the reciprocal Schmidt number, $1/S_c$, defined as

$$S_c = \frac{\epsilon_m}{\epsilon_c} \tag{22}$$

where ϵ_m and ϵ_c are eddy diffusivities of momentum and mass diffusion, respectively. The time-dependent particle dispersion functions for various Stokes numbers are plotted in Figures 6a to 6c. In general, more variations in dispersion function are noted for particles of smaller Stokes numbers as shown in Figure 6a, because their dispersions are closely influenced by the large-scale structures, which undergo continuous change. Initially, fluid particles (St = 0.1) disperse faster, but as particles of larger Stokes number gradually adjust to the fluid stream, they first catch up with the fluid particles in dispersion rate and then exceed the fluid particles as they start to get flung out of the vortex structures. This is further verified by the higher dispersion rate of particles with St = 1 than those with St = 0.5 after $T > 40$. On the larger Stokes number side the dispersion functions all vary smoothly with T^2, as indicated in Figure 6c for Stokes numbers of 50 or larger. This result for large Stokes number particles is similar to that predicted by Hinze (1975) for particle dispersion in homogeneous turbulent flows. For particles with large Stokes number, the scale of the vortex structure in a mixing layer becomes relatively small as the residence time of these high-inertia particles in the vortex structures is short. The large-scale structures resemble homogeneous turbulence for large Stokes number particles. The particle dispersion functions for particles with Stokes numbers ranging between the two extreme groups are shown in Figure 6b. It is clear that the dispersion of this group represents the transition from low to high Stokes numbers.

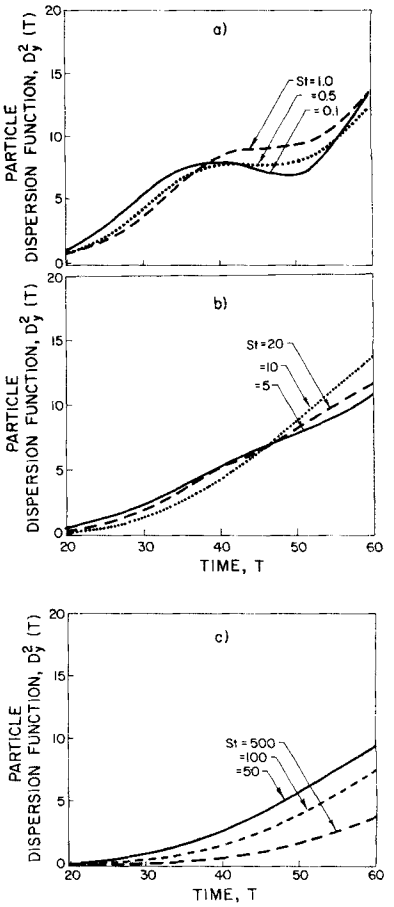

Figure 6. Particle dispersion function as a function of time.

Other interesting information is presented in Figure 7 for the maximum value of γ_D between $T = 0$ and 60 as a function of the Stokes number. Again it is confirmed that there is a range of Stokes numbers where the dispersion of particles is larger than the fluid. In this study, since only the large-scale structures and their interaction are modeled, we would caution that the dispersion results presented in this study are of the first order; second-order corrections, such as those due to small-scale modulation and forces other than the drag forces were not included.

Conclusions

Numerical simulations of the particle dispersion in a plane mixing layer are presented. The two-dimensional free shear flow is modeled through a discrete vortex method. Qualitatively the discrete vortex simulations compare favorably with available experimental results regarding global flow patterns, vortex interactions, and the pairing process. The predicted mean velocities, velocity similarity, and momentum thickness are comparable with measured values.

For particle dispersion simulations, it was found that in general the mixing layer is capable of dispersing the particles beyond the boundary of the fluid dispersion for those particles with Stokes numbers of the order of unity. For small Stokes numbers, the particle dispersion resembles that of the fluid particles while for large Stokes numbers the dispersion decreases with increasing Stokes number. For particles introduced to the flow from the low-speed side and near the tip of the splitter plate, the dispersion and mixing are more extensive and persistent than those of particles entering the flow from the high-speed side. This is due to the differences in local intrinsic Stokes numbers. Qualitatively, the time-dependent particle dispersion function also confirms the dispersion trend that, for intermediate Stokes numbers, the particle dispersion rate is larger than that of the fluid. For very large Stokes number the dispersion function is proportional to T^{-2}, which was previously reported for particle dispersion in homogeneous turbulent flows. The results of this simulation indicate that there seems to exist a specific range of intermediate Stokes number at which optimal dispersion of particles in a turbulent mixing layer may be achieved.

Acknowledgment

Numerical computation was made possible through a grant of computer time from the Computer Center of Washington State University. R. Chein was supported as a teaching assistant by the Department of Mechanical and Materials Engineering, Washington State University.

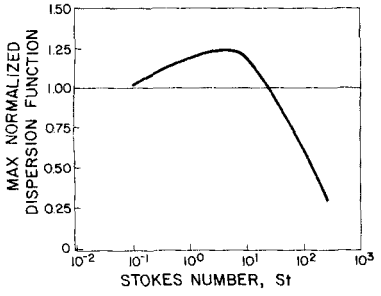

Figure 7. Maximum normalized particle dispersion $\gamma_{D_{max}}$ vs. Stokes number.

Notation

d_p = particle diameter
$D_p^2(T)$ = particle dispersion function
$D_{fp}^2(T)$ = fluid particle dispersion function
f = correction factor for non-Stokes drag
L = unit length
l = spacing of vortex array
$N(T)$ = total number of particles in flow field at time T
N_b = total number of vortices in vortex array
N_m = total number of vortices in mixing layer
Re_f = flow Reynolds number
Re_p = particle Reynolds number
r/D = dimensionless round jet radius
S_c = Schmidt number
St = particle Stokes number
t = dimensional time
T = new dimensionless time = $\tau - 120$
u_1 = free stream velocity of high-speed side of mixing layer
u_2 = free stream velocity of low-speed side of mixing layer
$\overline{u}$ = unit velocity
U_1 = dimensionless free stream velocity of high-speed side of mixing layer
U_2 = dimensionless free stream velocity of low-speed side of mixing layer
u_c = average velocity of mixing layer = $\frac{1}{2}(u_1 + u_2)$
(U, V) = dimensionless flow velocity vector
$\vec{v}$ = dimensional flow velocity vector
$\vec{v}_p$ = dimensional particle velocity vector
$W(Z)$ = complex potential, Eq. 6
(X, Y) = dimensionless coordinates vector
Y_m = mean particle displacement in y direction
Z = complex coordinate = $X + iY$

Greek letters

α = free stream velocity ratio = U_2/U_1
Δu = velocity difference = $u_1 - u_2$
ΔU = dimensionless velocity difference = $U_1 - U_2$
Δt = dimensional time step size
$\Delta\tau$ = dimensionless time step size
ϵ_m = eddy diffusivity of momentum
ϵ_c = eddy diffusivity of mass
Γ = vortex strength per unit length of vortex sheet
γ_d = dimensionless particle size
γ_ρ = density ratio = ρ_p/ρ
γ_D = ratio of particle dispersion function to fluid dispersion function
λ = system parameters = $(U_1 - U_2)/(U_1 + U_2)$
μ = fluid dynamic viscosity
ν = fluid kinematic viscosity
ρ = fluid density
ρ_p = particle density
σ = cutoff radius of a vortex core
ψ = stream function
τ = dimensionless time

Literature Cited

Acton, E., "A Modeling of Large Eddies in an Axisymmetric Jet," *J. Fluid Mech.*, **98,** 31 (1980).

Batchelor, G. K., "Diffusion on Free Turbulent Shear Flows," *J. Fluid Mech.*, **3,** 67 (1956).

Brown, G. L., and A. Roshko, "On Density Effects and Large Structure in Turbulent Mixing Layers," *J. Fluid Mech.*, **64,** 775 (1974).

Chein, R., "Momentum Transport and Particle Dynamics in Turbulent Shear Flows," Ph.D. Thesis, Dept. Mech. Matls. Eng., Washington State University (1986).

Chein, R., and J. N. Chung, "Effects of Vortex Pairing on Particle Dispersion in Turbulent Shear Flows," *Int. J. Multiph. Flow,* **13,** 785 (1987).

Chorin, A. J., "Numerical Study of Slightly Viscous Flow," *J. Fluid Mech.*, **57,** 785 (1973).

Chung, J. N., and T. R. Troutt, "Simulation of Particle Dispersion in a Jet," *J. Fluid Mech.*, **186,** 199 (1988).

Crowe, C. T., "Review—Numerical Models for Dilute Gas Particle Flows," *ASME J. Fluids Eng.*, **104,** 297 (1982).
Crowe, C. T., R. A. Gore, and T. R. Troutt, "Particle Dispersion by Coherent Structures in Free Shear Flows," *Particle Sci. Technol.*, **3,** 149 (1985).
Elghobashi, S. E., and T. W. Abou-Arab, "A Two-Equation Turbulence Model for Two-Phase Flows," *Phys. Fluids,* **25,** 931 (1983).
Field, M. A., BCURA Members Info. Circular No. 273 (1963).
Goldschmidt, V. W., and S. Eskinazi, "Two-Phase Turbulent Flow in a Plane Jet," *J. Appl. Mech.*, **33,** 1 (1966).
Goldschmidt, V. W., M. K. Householder, G. Ahmadi, and S. C. Chuang, "Turbulent Diffusion of Small Particles Suspended in Turbulent Jets," *Prog. Heat Mass Trans.*, **6,** 487 (1972).
Gore, R. A., C. T. Crowe, T. R. Troutt, and J. J. Riley, "A Numerical Study of Particle Dispersion in Large-Scale Structures." *ASME Pub. HTD-47, Multiphase Flow and Heat Transfer,* BK No. 600304 (1985).
Hinze, J. O., *Turbulence,* 2nd ed. McGraw-Hill, New York (1975).
Householder, M. K., and V. W. Goldschmidt, "Turbulent Diffusion and Schmidt Number of Particles," *Proc. ASCE Eng. Mechanics Div.,* **EM6,** 1345 (1969).
Inoue, O., "Vortex Simulation of a Turbulent Mixing Layer," *AIAA J.,* **23** (3), 367 (1985).
Laitone, J. A., "A Numerical Solution for Gas-Particle Flow at High Reynolds Numbers," *J. Appl. Mech.*, **48,** 465 (1981).
Leonard, A., "Vortex Methods for Flow Simulation," *J. Comput. Phy.*, **37,** 289 (1980).
Lilly, G. P., "Effect of Particle Size on Particle Eddy Diffusivity," *Ind. Eng. Chem. Fundam.*, **12,** 268 (1973).
Memmot, V. J., and L. D. Smoot, "Cold Flow Mixing Rate Data for Pulverized Coal Reactors," *AIChE J.*, **24,** 466 (1978).
Mostafa, A. A., and S. E. Elghobashi, "A Two-Equation Turbulence Model for Jet Flows Laden with Vaporizing Droplets," *Int. J. Multiph. Flow,* **11,** 515 (1985).
Oster, D., and I. Wynanski, "The Forced Mixing Layer between Parallel Streams," *J. Fluid Mech.*, **123,** 90 (1982).
Rosenhead, L., "Formulation of Vortices from a Surface of Discontinuity," *Proc. Roy. Soc. London A,* **134,** 170 (1932).
Roshko, A., "Structures of Turbulent Flows, A New Look," *AIAA J.,* **14,** 1349 (1976).
Sheun, J. S., L. D. Chen, and G. M. Faeth, "Evaluation of a Stochastic Model of Particle Dispersion in a Turbulent Round Jet," *AIChE J.,* **29** (1), 167 (1983).
Shuen, J. S., A. S. P. Solomon, Q. F. Zhang, and G. M. Faeth, "Structure of Particle-Laden Jets: Measurements and Predictions," *AIAA J.*, **23,** 396 (1985).
Winant, C. D., and F. K. Browand, "Vortex Pairing, The Mechanism of Turbulent Mixing Layer Growth at Moderate Reynolds Numbers," *J. Fluid Mech.*, **63,** 237 (1974).
Yuu, S., N. Yasukouchi, Y. Hirosawa, and T. Jotaki, "Particle Turbulent Diffusion in a Dust-Laden Round Jet," *AIChE J.*, **24,** 509 (1978).

Manuscript received Nov. 17, 1986, and revision received Dec. 29, 1987.